Toward an integrated device for spatiotemporal superposition of free-electron lasers and laser pulses

Riccardo Mincigrucci,[1,*] Alessia Matruglio,[2,3,9] Andrea Calvi,[4] Laura Foglia,[1] Emiliano Principi,[1] Alberto Simoncig,[1] Filippo Bencivenga,[1] Stefano Dallorto,[5,6,7] Alessandro Gessini,[1] Gabor Kurdi,[1] Deirdre Olynick,[5] Scott Dhuey,[5] Rudi Sergo,[8] Marco Lazzarino,[2] Claudio Masciovecchio,[1] and Simone Dal Zilio[2,10]

[1]Elettra Sincrotrone Trieste, Area Science Park Basovizza S.S. 14 Km 163.5, Trieste 34149, Italy
[2]IOM Laboratorio Nazionale TASC, CNR, Area Science Park Basovizza S.S. 14 Km 163.5, Trieste 34149, Italy
[3]Graduate School in Nanotechnology, University of Trieste, Piazzale Europa 1, Trieste 34127, Italy
[4]Dipartimento di Fisica, Università degli Studi di Trieste, via A. Valerio 2, I-34127 Trieste, Italy
[5]Molecular Foundry, 1 Cyclotron Road, Berkeley, California 94720, USA
[6]Department of Micro- and Nanoelectronic Systems, Institute of Micro and Nanoelectronics, Faculty of Electrical Engineering and Information Technology, Ilmenau University of Technology, Gustav-Kirchhoff-Straße 1, Ilmenau 98693, Germany
[7]Oxford Instruments, 300 Baker Avenue, Suite 150, Concord, Massachusetts 01742, USA
[8]Detector and Instrumentation Laboratory, Elettra Sincrotrone Trieste, Area Science Park Basovizza S.S. 14 Km 163.5, Trieste 34149, Italy
[9]e-mail: matruglio@iom.cnr.it
[10]e-mail: dalzilio@iom.cnr.it
*Corresponding author: riccardo.mincigrucci@elettra.eu

Free-electron lasers (FELs) currently represent a step forward on time-resolved investigations on any phase of matter through pump-probe methods involving FELs and laser beams. That class of experiments requires an accurate spatial and temporal superposition of pump and probe beams on the sample, which at present is still a critical procedure. More efficient approaches are demanded to quickly achieve the superposition and synchronization of the beams. Here, we present what we believe is a novel technique based on an integrated device allowing the simultaneous characterization and the fast spatial and temporal overlapping of the beams, reducing the alignment procedure from hours to minutes.   © 2016 Optical Society of America

Time-resolved investigations have begun a new era of chemistry and physics, enabling the monitoring in real time of the dynamics of chemical reactions and matter [1]. Generally, in such kinds of studies, one or more laser pulses acts as the pump, triggering a particular process such as ultrafast melting [2,3], demagnetization dynamics [4,5], impulsive stimulated scattering [6,7], and coherent antiStokes Raman scattering [8–10], to name a few. The particular dynamics triggered by the pump pulse is then probed by another laser pulse which, properly delayed, encodes the temporal information of the process (e.g., in the scattered intensity). The physical information is thus contained in the temporal trace of the monitored physical quantity obtained by varying the pump-probe delay. A further step in time-resolved investigations has been achieved with the advent of free-electron lasers (FELs), which permitted the addition of chemical and elemental selectivity to the above-mentioned studies [11–13]. In general, any pump-probe study requires the spatial and temporal superposition of the pump and probe lasers, which is realized by exploiting the peculiar properties of different samples. In particular, in the FEL-optical laser class of experiments, the first step is the spatial superposition of the two beams, which is usually accomplished using a cerium-doped yttrium aluminum (Al) garnet fluorescent screen (YAG:Ce); the FEL-induced fluorescence is used to define the FEL position on the sample to which the optical laser is subsequently superposed. We have already presented a novel pixeled phosphor detector (PPD), which allows an improvement with respect to standard YAG as far as FEL diagnostics is concerned [14]. Once the spatial superposition has been achieved, the YAG is substituted with an antenna [15] coupled with an oscilloscope and used to roughly align the two pulses in time. This superposition is conducted looking at the electrical signals generated by the FEL and the laser; the relative delay is adjusted until the rising edges of the two are overlapped. This procedure is quite

inaccurate, and the delay value can be determined only with a 30 ps error, a value that is dictated by the intrinsic temporal resolution of the common oscilloscopes. The subpicosecond synchronization requires a much faster diagnostic, and the finer temporal superposition is subsequently conducted using a third sample (e.g., Si_3N_4 or Al_2O_3 crystals) and monitoring the FEL-induced changes in the visible/IR optical properties. In insulators and semiconductors, the main process, which underlies the optical property changes, is believed to be a partial depletion of the valence band, resulting in an induced absorption [16]; the imaginary part "k" of the refractive index increases, and this should manifest in a diminished reflection and/or transmission, accompanied by a perturbation of the value of the real part of the refractive index, which can cause an interferential demagnification of the transient signal [17,18]. The overall procedure is generally time-consuming and highly complex. Each sample is employed for its peculiar characteristics, and only for a specific task of the overall alignment procedure. This is inefficient and not robust. First of all, the spatial superposition has to be preserved during the temporal alignment steps. This is commonly obtained by using as a reference the image of a CCD camera; after the spatial superposition, the CCD is put in focus and thus every subsequent sample has to be adjusted in order to reach the same level of focus. The quality of the focus is defined by a human user and is influenced by the quality of the sample surface, by the illumination, and by the geometry of the imaging setup. A second and more substantial problem in the alignment procedure is represented by the scarce contrast of the transient signal; since the FEL spot can be smaller than the laser spot, the valence band is depleted by the FEL radiation only in a fraction of the sample surface. Therefore, a fraction of the visible laser is reflected or transmitted by an unexcited sample, giving rise to a dominant baseline over which to detect the transient signal. We propose here a beam monitor designed to increase the contrast and to speed up the alignment procedure. The ideal sample should possess the fluorescence characteristics of a YAG screen and at the same time be suitable for the temporal overlapping procedure with an increased contrast. This can be obtained, for example, by embedding some Al_2O_3 timing zones in a modified version of the PPD previously proposed by our group [14]; we call this enhanced version PPD 2.0. This new device would permit employing adjacent portions of the same surface to spatially (using the phosphors pixels) and temporally (using the Al_2O_3 islands) superpose the FEL and laser beams. A simple strategy to drastically increase the contrast is to operate in transmission (thus looking for a change in transmittivity induced by the FEL pulse) and to create a pinhole around the Al_2O_3 zones. The pinhole, realized by a reflective material for the visible/IR laser, should be smaller or comparable to the FEL beam size. This permits geometrically blocking the circular crown of the laser spot that would not interact with the FEL-excited portion of the Al_2O_3, avoiding the origin of baseline contribution, as shown in the sketch in Fig. 1. A scheme of the fabrication process of such a sample is reported in Fig. 2; in detail, a fused silica wafer (250 μm thick) is coated with 50 nm thick chromium (Cr) thin film via e-beam evaporation and with 400 nm of ZEP 520A resist for the following lithography. The micrometric honeycomb pattern is achieved by direct e-beam lithography (EBL) at 200 kV and 1 nA using a Vistec VB-300 EBL system [Fig. 2(a)]. Cr wet etching is used for pattern transfer on a metal mask. For the transfer in the silica substrate, a plasma etching process is carried out with a multiple
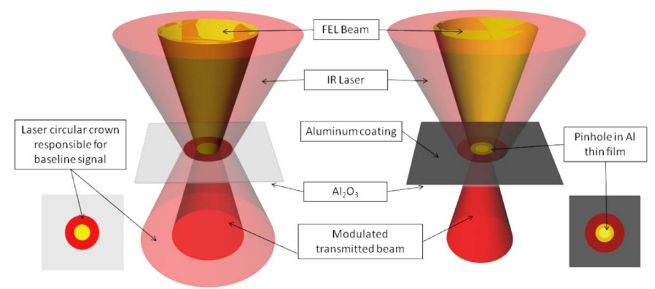

Fig. 1. Left part: sketch of usual superposition between the laser and FEL spots. The circular crown of the laser spot not excited by the FEL produces a nonnegligible baseline. Right part: the introduction of a pinhole equal or smaller than the FEL spot cuts the unexcited circular crown, increasing the contrast.
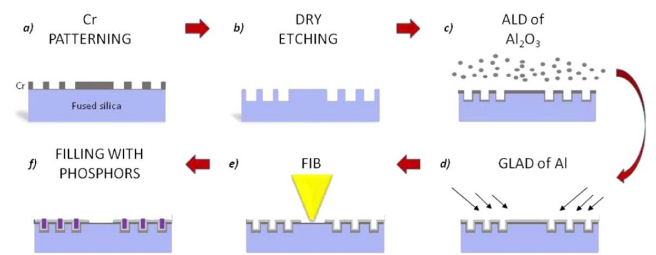

Fig. 2. Scheme of the fabrication process. (a) EBL on Cr-coated fused silica; (b) dry etching of fused silica; (c) ALD of Al_2O_3; (d) GLAD deposition of Al; (e) FIB process; (f) phosphor deposition.

frequency parallel plate etching tool with 60 MHz on the top plate and 13.56 MHz on the bottom plate (Oxford Plasma lab 100 Viper). The periodic lattice of micrometric pixels is etched through 4 μm of fused silica with a mixture of 70 sccm CF4 40% O_2 at 20 mTorr of pressure, 150 W of radio-frequency power and 400 W VHF forward power [Fig. 2(b)]. The diameter and period of holes are 2 μm and 4 μm, respectively, with a total fill factor of an active area close to 20%. After the etching step, the surface is covered with a 250-nm-thick Al_2O_3 deposited by plasma-enhanced atomic layer deposition (ALD) at 40°C (Oxford FlexAl) [Fig. 2(c)]. After that, a conformal layer of 100 nm of Al is evaporated on the sample by the Glancing Angle Deposition (GLAD) process [Fig. 2(d)]; the metal thin film is needed to reduce the cross talk between the pixels of phosphor and to achieve the desired pinhole structures where the visible/IR laser is transmitted. The patterning of the Al layer is performed by selectively removing the metal layer, avoiding the damaging of Al_2O_3 under the layer by the focused ion beam (FIB) process [Fig. 2(e)]. The final step is the deposition of phosphors inside the 2 μm cavities [Fig. 2(f)]; the process is described in Ref. [14]. The P20 used phosphor is commercially available at Phosphor Technology Company. Scanning electron microscopy (SEM) images of the sample before [Fig. 3(a)] and after the phosphors' deposition [Fig. 3(b)] are presented. The average grain size of powder ranges from a minimum of 1.2 μm to a maximum of 6 μm, as reported by the company. The 2 μm holes are thus fillable only with a small fraction of the available grains. This causes an incomplete filling and a decrease in the FEL-visible conversion efficiency. After the fabrication, the sample was installed and tested at the EIS-TIMEX beam line [19], at the FERMI FEL facility
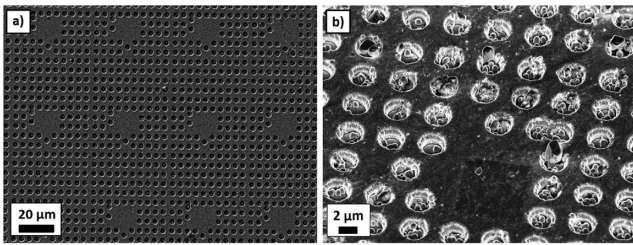
Fig. 3. SEM images of the device. (a) Before FIB and the filling with phosphors; (b) after phosphor deposition. An Al_2O_3 island and the phosphor presence can be noticed in the microcavities.

in Trieste, Italy. The beam line is conceived to operate pump-probe experiments in a high-fluency regime both for the FEL and IR laser. For this purpose, it is equipped on the FEL side with an ellipsoidal gold-coated mirror able to focus the FEL emission down to 6 μm at full width half maximum (FWHM). In such conditions, the FEL is generally destructive, an undesired feature as far as the overlapping procedure is concerned. The superposition is thus conducted out of the focal plane of the FEL, where the spot has a dimension of 15 μm, and decreases the intensity at the source down to 1 μJ. In the present case, the FEL wavelength was 32 nm. The employed IR laser had a FWHM of 50 μm and an intensity of 0.1 μJ. Figure 4 (upper part) reports a schematic of the experimental setup. The sample was rotated by 20° with respect to the FEL beam, due to a mechanical constraint of the manipulator. The spatial overlap was conducted in such rotated geometry. The bottom part of Fig. 4 shows the images of the spots acquired for the FEL and the IR on the above described sample. The images have been acquired using a Questar QM 100 telemicroscope, operated in air and coupled to a Basler ACE CCD camera.

By comparing the images, it is easy to observe that the laser spot is roughly twice as large as the FEL spot. The inhomogeneous readout of the FEL spot intensity is due to
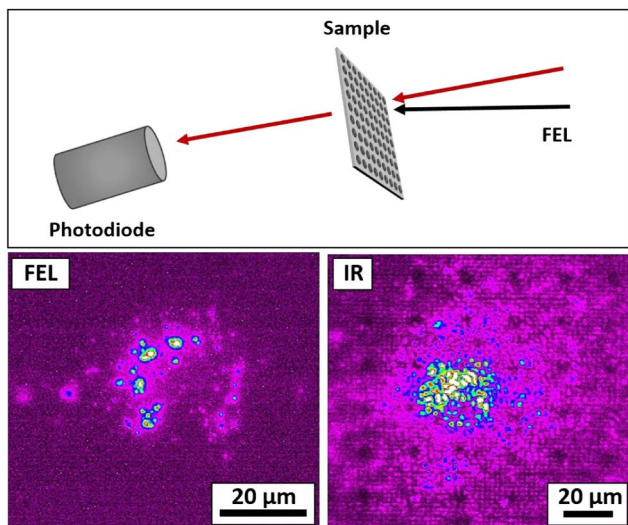

Fig. 4. Upper part: sketch of the experimental apparatus. Lower part: FEL spot (on the left) and IR laser spot (on the right). A lack of luminosity in the lower right part of both the spots identifies the presence of an Al_2O_3 timing zone (represented also in the SEM image in the inset). The images were obtained using a Questar QM100 telemicroscope operated in air and coupled to a CCD camera.

the incomplete filling of the phosphor holes: it is also possible to recognize on the lower/right part the lack of intensity of the spot that corresponds to the unpatterned area of the Al_2O_3 timing island. The fine-timing procedure was subsequently conducted monitoring the time evolution of the transmittivity of the Al_2O_3-excited island. An UVG100 (OptoDiode) photodiode was employed to detect the transmitted IR intensity. Figure 5 reports the relative change of transmittivity of our device (red trace) and, for comparison, the one recorded on the bulk Al_2O_3 (black trace) and on a 100 nm Ni-coated bulk Al_2O_3 (blue trace). All the measurements were conducted under the same FEL and laser conditions. To obtain the traces shown in Fig. 5, the delay between the IR and FEL laser was continuously increased and the shot-to-shot transmitted intensity was recorded. This procedure was repeated three times for each sample, and the single traces have been averaged and binned with 20 fs steps. The error bars are one standard error. The bulk Al_2O_3 exhibits a change of the transmittivity in the order of a few percent, comparable with the standard timing traces generally reported in the literature [18,20].

In contrast, on our device the transmittivity change is amplified by cutting the fraction of the IR that does not interact with the excited region of the sample. As expected, this increases the intensity of the effect up to ∼25%. The blue trace is instead obtained on a nominally identical Al_2O_3 sample coated with 100 nm of Ni. The coating is removed by exposing the sample to an unattenuated FEL. The high-intensity FEL drills a hole of its dimensions, which can subsequently be used as an Al_2O_3 island to perform the fine timing with an attenuated FEL. Such a procedure is a valid alternative that also produces a contrast increase with respect to the uncoated bulk sample, but does not possess the capabilities for the spatial alignment offered by the PPD approach.

In conclusion, we have determined two different procedures to solve the identified common problems responsible for the scarce contrast in the temporal overlapping procedure of the FEL and laser pulses: the introduction of a metallic coating, subsequently removed by a high-intensity FEL, and the creation of a purposely designed sample with well-defined pinholes. The PPD 2.0 permits an increase in the contrast by a factor
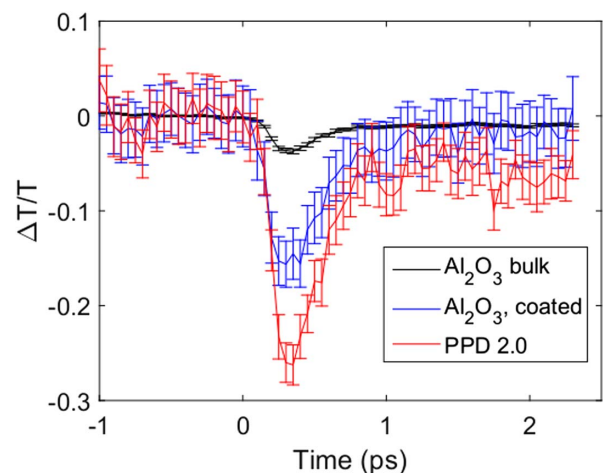

Fig. 5. Fine-timing traces acquired on the same FEL/IR laser condition on three different samples: bulk Al_2O_3 (black trace), Ni-coated bulk Al_2O_3 (blue trace), and our sample (red trace).

$\sim$7 with respect to the bulk Al_2O_3 crystal, being contemporarily exploitable for the spatial overlapping procedure. This allows more efficiency in the overall superposition procedure in terms of time and spatial precision, since it does not require the use of different crystals with their own characteristics. The integration of currently used tools can be pushed further with the introduction of an electric contact on the surface coating; that would allow operating our sample as the antenna described in Refs. [15,21] and also conducting the raw-timing procedure on the same spot. Specific setups exploiting high-resolution spatial detection devices can be employed to have even higher contrast in the timing signal. However, such types of setups have to be carefully designed and aligned to detect the reflected or transmitted signal [22–24]. Instead, our device can be fruitfully inserted in any existing transmission setup, achieving at the same time an increase in the available space and an augmented contrast in the timing signal. The geometrical parameters of the PPD 2.0, such as relative distances, diameters, and depths, can be easily modified to extend its use toward noncollinear geometries, where small spatial deviations between the YAG screen and the timing sample may also become important. An increase of the cavities' diameter may also bring an efficiency increase due to an augmented filling factor. It is important to have a compromise between the filling of the cavities and their size: large diameters (tens of μm) reduce the resolution in the diagnostic of the FEL beam; a diameter of 4 μm can be a good compromise with this type of phosphors, as already demonstrated by our group. Moreover, as far as the linear absorption process holds for the timing material [22], our device can be employed with identical advantages in terms of contrast increase and speeding up the overall procedure. The only constraint is regarding the dimensions of the timing islands, which have to be rescaled according to the adopted FEL focal spot size. A study on different materials that change their optical properties when exposed to the FEL beam, such as Si_3N_4, GaAs, MgF_2, or wide bandgap insulators could be interesting to determine the best material to further increase the contrast and in principle speed up the overlapping procedure.

REFERENCES

1. A. H. Zewail, in Nobel Lectures in Chemistry, I. Grethe, ed. (1996–2000).
2. M. Beye, F. Sorgenfrei, W. F. Schlotter, W. Wurth, and A. Föhlisch, Proc. Natl. Acad. Sci. USA **107**, 16772 (2010).
3. N. Medvedev, Z. Li, and B. Ziaja, Phys. Rev. B **91**, 1 (2015).
4. B. Vodungbo, B. Tudu, J. Perron, R. Delaunay, L. Müller, M. H. Berntsen, G. Grübel, G. Malinowski, C. Weier, J. Gautier, G. Lambert, P. Zeitoun, C. Gutt, E. Jal, A. H. Reid, P. W. Granitzka, N. Jaouen, G. L. Dakovski, S. Moeller, M. P. Minitti, A. Mitra, S. Carron, B. Pfau, C. von Korff Schmising, M. Schneider, S. Eisebitt, and J. Lüning, Sci. Rep. **6**, 18970 (2016).
5. C. Von Korff Schmising, M. Giovannella, D. Weder, S. Schaffert, J. L. Webb, and S. Eisebitt, New J. Phys. **17**, 033047 (2015).
6. Y.-X. Yan, E. B. Gamble, Jr., and K. A. Nelson, J. Chem. Phys. **83**, 5391 (1985).
7. S. Fujiyoshi, S. Takeuchi, and T. Tahara, J. Phys. Chem. A **107**, 494 (2003).
8. F. El-Diasty, Vib. Spectrosc. **55**, 1 (2011).
9. G. Knopp, P. Radi, M. Tulej, T. Gerber, and P. Beaud, J. Chem. Phys. **118**, 8223 (2003).
10. H. U. Stauffer, J. D. Miller, M. N. Slipchenko, T. R. Meyer, B. D. Prince, S. Roy, and J. R. Gord, J. Chem. Phys. **140**, 024316 (2014).
11. S. Tanaka and S. Mukamel, J. Chem. Phys. **116**, 1877 (2002).
12. S. Tanaka and S. Mukamel, Phys. Rev. Lett. **89**, 043001 (2002).
13. S. Mukamel and S. Tanaka, Phys. Rev. A **64**, 032503 (2001).
14. A. Matruglio, S. Dal Zilio, R. Sergo, R. Mincigrucci, C. Svetina, E. Principi, N. Mahne, L. Raimondi, A. Turchet, C. Masciovecchio, M. Lazzarino, G. Cautero, and M. Zangrando, J. Synchrotron Radiat. **23**, 29 (2016).
15. M. B. Danailov, F. Bencivenga, F. Capotondi, F. Casolari, P. Cinquegrana, A. Demidovich, E. Giangrisostomi, M. P. Kiskinova, G. Kurdi, M. Manfredda, C. Masciovecchio, R. Mincigrucci, I. P. Nikolov, E. Pedersoli, E. Principi, and P. Sigalotti, Opt. Express **22**, 12869 (2014).
16. S. M. Durbin, AIP Adv. **2**, 042151 (2012).
17. F. Casolari, F. Bencivenga, F. Capotondi, E. Giangrisostomi, M. Manfredda, R. Mincigrucci, E. Pedersoli, E. Principi, C. Masciovecchio, and M. Kiskinova, Appl. Phys. Lett. **104**, 191104 (2014).
18. S. Eckert, M. Beye, A. Pietzsch, W. Quevedo, M. Hantschmann, M. Ochmann, M. Ross, M. P. Minitti, J. J. Turner, S. P. Moeller, W. F. Schlotter, G. L. Dakovski, M. Khalil, N. Huse, and A. Föhlisch, Appl. Phys. Lett. **106**, 061104 (2015).
19. C. Masciovecchio, A. Battistoni, E. Giangrisostomi, F. Bencivenga, E. Principi, R. Mincigrucci, R. Cucini, A. Gessini, F. D'Amico, R. Borghes, M. Prica, V. Chenda, M. Scarcia, G. Gaio, G. Kurdi, A. Demidovich, M. B. Danailov, A. Di Cicco, A. Filipponi, R. Gunnella, K. Hatada, N. Mahne, L. Raimondi, C. Svetina, R. Godnig, A. Abrami, and M. Zangrando, J. Synchrotron Radiat. **22**, 553 (2015).
20. C. Gahl, A. Azima, M. Beye, M. Deppe, K. Döbrich, U. Hasslinger, F. Hennies, A. Melnikov, M. Nagasono, A. Pietzsch, M. Wolf, W. Wurth, and A. Föhlisch, Nat. Photonics **2**, 165 (2008).
21. L. Raimondi, C. Svetina, N. Mahne, D. Cocco, A. Abrami, M. De Marco, C. Fava, S. Gerusina, R. Gobessi, F. Capotondi, E. Pedersoli, M. Kiskinova, G. De Ninno, P. Zeitoun, G. Dovillaire, G. Lambert, W. Boutu, H. Merdji, A. I. Gonzalez, D. Gauthier, and M. Zangrando, Nucl. Instrum. Methods Phys. Res. A **710**, 131 (2013).
22. R. Riedel, A. Al-Shemmary, M. Gensch, T. Golz, M. Harmand, N. Medvedev, M. J. Prandolini, K. Sokolowski-Tinten, S. Toleikis, U. Wegner, B. Ziaja, N. Stojanovic, and F. Tavella, Nat. Commun. **4**, 1731 (2013).
23. S. Schorb, T. Gorkhover, J. P. Cryan, J. M. Glownia, M. R. Bionta, R. N. Coffee, B. Erk, R. Boll, C. Schmidt, D. Rolles, A. Rudenko, A. Rouzee, M. Swiggers, S. Carron, J. C. Castagna, J. D. Bozek, M. Messerschmidt, W. F. Schlotter, and C. Bostedt, Appl. Phys. Lett. **100**, 121107 (2012).
24. T. Maltezopoulos, S. Cunovic, M. Wieland, M. Beye, A. Azima, H. Redlin, M. Krikunova, R. Kalms, U. Frühling, F. Budzyn, W. Wurth, A. Föhlisch, and M. Drescher, New J. Phys. **10**, 033026 (2008).